Journal of Control, Automation and Electrical Systems (2021) 32:796–806
https://doi.org/10.1007/s40313-021-00708-x

Closed-Form Approximation for Grounding Grids Transient Analysis

Rodolfo Antônio Ribeiro de Moura[1] · Marco Aurélio de Oliveira Schroeder[1] · Antonio Carlos Siqueira de Lima[1] · Pedro Henrique Nascimento Vieira[1] · Rafael Alipio[1]

Received: 27 June 2020 / Revised: 6 January 2021 / Accepted: 20 February 2021 / Published online: 15 March 2021
© Brazilian Society for Automatics–SBA 2021

Abstract
Traditionally, wideband modeling of grounding system demands the usage of the method of moments (MoM) which implies a large number of segments to represent the conductors involved and the solution of a double integral for each and every one of these segments. Approaches presented in the literature as PEEC (partial element equivalent circuit) and HEM (hybrid electromagnetic model) are based on these assumptions. In either of these approaches, a heavy computational burden occurs, leading to a very time-consuming simulation. This paper proposes to use a two-term series expansion to allow a closed-form solution to the double integral found in HEM and thus is named as sHEM. The proposed approach, sHEM, is compared with HEM with respect to the harmonic impedance and the time responses associated with impulse currents. The results indicate only a small loss of accuracy with respect to the peak value of the overvoltage with a significant gain in the computational time. Finally, a comparison with actual measurement results is provided to evaluate the adequacy of using sHEM in the analysis of grounding grids.

Keywords Grounding · MacLaurin series · Method of moments · Numerical analysis · Transient analysis

1 Introduction

For an accurate assessment of the transient response of grounding system, a wideband representation of all elements involved is commonly required. In this scenario, the frequency range of interest goes from a few hertz up to tenths of MHz. A detailed representation is warranted by using approaches such as the finite differences time domain (FDTD) Tanabe (2001), Tsumura et al. (2006), Yamamoto et al. (2010)), finite element method (FEM) Akbari et al. (2013) and method of moments (MoM) Grcev and Dawalibi (1990), Visacro and Portela (1992), Visacro and Soares (2005), the last two developed in the frequency domain. Considering full-wave frequency-domain techniques, MoM is probably the most used approach as it solves the associated integral equation by dividing all conductors in very small segments. There are essentially two approaches to do so. The first one relies on deriving directly a generalized impedance matrix from the tangential electric field at the conductor surface (Grcev & Dawalibi, 1990), while the second consists in evaluating shunt and series impedance matrices and by using a suitable set of incidence matrices to obtain an equivalent nodal admittance matrix as in the so-called hybrid electromagnetic model (HEM) Visacro and Soares (2005) or in the partial element equivalent circuit (PEEC) Ruehli (1974, 1996) considering a lossy medium Yutthagowith et al. (2011). Regardless of the adopted approach, all methods present a heavy computational burden, thus demanding an improvement of their numerical performance.

The first attempt to improve the computational performance was to avoid the usage of MoM-based method altogether. For instance, uniform transmission line approximation Menter and Grcev (1994), non-uniform line modeling Liu et al. (2005) or representing the grounding system as a frequency-dependent network (FDNE) Lima et al. (2019) have been proposed in the literature. The latter approach has the disadvantage that demands the evaluation of the complete grounding system in the frequency range of interest although it avoids the burden of the inverse transform evaluation. The main computational burden of any MoM-based simulation lies in the large number of numerical integration of terms in the form of $\exp(-\gamma r)/r$ to be carried out at each frequency. Recently, some references have been pro-

✉ Rodolfo Antônio Ribeiro de Moura
moura@ufsj.edu.br

[1] Electrical Engineering Department, Federal University of São João del-Rei, Pa. Frei Orlando, 170 - Centro, São João del-Rei, MG 36307-352, Brazil

posed to modify the expression to be integrated, thus reducing the burden without a significant loss of accuracy. In Reference Grcev (2018), it is proposed to use the first term in the series expansion of the exponential term, while in Lima et al. (2019b) it is proposed to approximate the exponential term by an average thus removing it from the integration. This leads to a frequency-independent integration that can be calculated prior to entering the frequency domain loop. In Moura (2020), it is presented alternative solutions correspond to using approximations to the term $\exp(-\gamma r)/r$. Two approaches are considered either using MacLaurin series or Pad approximation. It is shown that the proposed solutions allow reducing the computational time, without jeopardizing accuracy. However, only horizontal electrodes were considered in this study.

This paper investigates the possibility of using the first two terms of MacLaurin series of $\exp(-\gamma r)/r$ in more complexes grounding grids, i.e., generalizing one of the two approaches existing in Moura (2020). This procedure also leads to a simplification of the integral which is then calculated using closed-form expression which present "geometrical terms," i.e., frequency-independent, and a very simple expression depending on the propagation constant. Given the fact that whole procedure is based upon a series expression the formulation presented in this paper is then named sHEM for series-HEM. To evaluate the adequacy and accuracy of the proposed formulation, several grounding grids were tested again. The results indicate a considerable gain; in some cases, the overall computation gain was close to 2,000 times faster than the conventional approach using HEM. It is worth mentioning that different grounding grid configurations have different computational performance to solve the linear system that depends uniquely on the number of segments. But the computational gain from using the proposed approach is consistent with any grounding grid configuration.

The paper is organized as follows: Sect. 2 presents the mathematical modeling of the grounding systems and the proposed approach. Section 3 presents the evaluation of the harmonic impedance for several configuration together with the comparison with the traditional HEM in order to assess the computational gain together with high precision of the proposed methodology. Time responses of the ground potential rise in both theoretical and actual configurations are used to assess the accuracy of the proposed approach. A discussion of the main advantages of sHEM together with some guidelines to how and when to apply it in a grounding system analysis is presented in Sect. 5. The main conclusions of this paper is presented in Sect. 6.

2 Mathematical Modeling

For the sake of clarity, we present a brief overview of HEM Visacro and Soares (2005). It is worth mentioning that the usage of HEM has increased significantly recently (Kuhar et al., 2017, 2018; CIGR, 2019; Schroeder et al., 2020). In fact, there has been a considerable set of experimental validations of HEM, e.g., Silveira et al. (2009), Visacro et al. (2011, 2015), Alipio (2017); Alipio et al. (2019)). The key aspect of HEM is the evaluation of shunt and series matrices associated with each segmented conductor. Either HEM or any method based on it such as its modified versions can deal with arbitrarily oriented conductors. However, as the main focus of this paper is in grounding grids where in most cases the conductors are either parallel or orthogonal, the development of the approximated expressions is based only for these two possible orientations. Thus, for instance, consider two orthogonal conductors in a general medium with conductivity σ, permittivity ε and permeability μ, where both σ and ε may present a frequency-dependent behavior. Figure 1 depicts this configuration where index "S" stands for the sending electrode and "R" for the receiving one, $\mathrm{d}l_R$ and $\mathrm{d}l_S$ are infinitesimal segments. The coordinates of the sending conductor are from (x_{S0}, y_{S0}, z_{S0}) to (x_{SI}, y_{SI}, z_{SI}), while for the receiving conductor they are from (x_{R0}, y_{R0}, z_{R0}) to (x_{RI}, y_{RI}, z_{RI}).

For the aforementioned configuration, one can then define a shunt impedance matrix $\mathbf{Z}_T$ associated with the transverse electromagnetic coupling and a series impedance matrix $\mathbf{Z}_L$ associated with the behavior of the electromagnetic field throughout the conductors. The expression for the shunt mutual impedance between conductors R and S is given by

$$Z_{T_{RS}} = \frac{1}{4\pi\,(\sigma + j\omega\varepsilon)\,\ell_S\,\ell_R} \int_{\ell_S}\int_{\ell_R} \frac{\exp(-\gamma r)}{r}\mathrm{d}l_R\mathrm{d}l_S \qquad (1)$$

while the series mutual impedance is then

$$Z_{L_{RS}} = -\frac{j\omega\mu}{4\pi} \int_{\ell_S}\int_{\ell_R} \frac{\exp(-\gamma r)}{r}\overrightarrow{\mathrm{d}l_R}\cdot\overrightarrow{\mathrm{d}l_S} \qquad (2)$$

where $\gamma = \sqrt{j\omega\mu\,(\sigma + j\omega\varepsilon)}$ is the propagation constant, r is the distance between infinitesimal segments, ℓ_S and ℓ_R are, respectively, the length of the conductor R and S, $\omega = 2\pi f$, f is the frequency of the signal, a is the radius of the electrode, and $\cdot$ stands for the scalar product.

For the expression for the self-elements, it is common to use a closed-form approximation as $\exp(-\gamma a) \approx 1$ and the expressions for the self-impedance proposed by Sunde (1968) can be used.

It is proposed to use a series approximation for the exponential term in (1) and (2). The first two terms in a MacLaurin

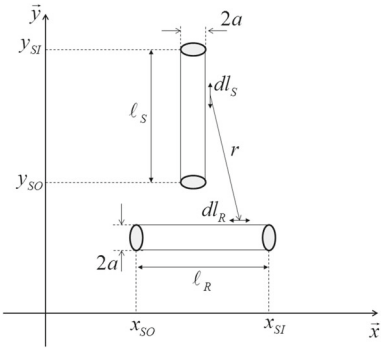

Fig. 1 Two orthogonal conductors in a uniform medium

series expansion are used; thus, the integrand can be rewritten as

$$\frac{\exp(-\gamma r)}{r} \approx \frac{1}{r} - \gamma \tag{3}$$

Using (3) in (1) and (2) allows a closed-form solution for line integrals. Thus, it is possible to approximate $Z_{T_{RS}}$ and $Z_{L_{RS}}$ by

$$\begin{aligned} Z_{T_{RS}} &= \frac{1}{4\pi(\sigma + j\omega\varepsilon)} \frac{m_A + m_B + m_C}{\ell_S \ell_R} \\ Z_{L_{RS}} &= -\frac{j\omega\mu}{4\pi}(m_A + m_B + m_C) \end{aligned} \tag{4}$$

where m_A, m_B and m_C are shown below in (5) to (7) where it is assumed that $x_{RO} = x_{RI} = x_R$ and $y_{SO} = y_{SI} = y_S$, ensuring that both segments are indeed orthogonal. Both m_A and m_B can be understood as "geometrical constants" of a given configuration and are then frequency independent, while m_C is a simple function of γ.

$$\begin{aligned} m_A = {} & (x_{SO} - x_R) \\ & \times \ln\left(\left|\sqrt{a^2 + (x_R - x_{SO})^2 + (y_{RO} - y_S)^2} + y_{RO} - y_S\right|\right) \\ & + (y_{RO} - y_S) \\ & \times \ln\left(\left|\sqrt{a^2 + (x_R - x_{SO})^2 + (y_{RO} - y_S)^2} - x_R + x_{SO}\right|\right) \\ & + (x_R - x_{SO}) \\ & \times \ln\left(\left|\sqrt{a^2 + (x_R - x_{SO})^2 + (y_{RI} - y_S)^2} + y_{RI} - y_S\right|\right) \\ & + (y_S - y_{R1}) \\ & \times \ln\left(\left|\sqrt{a^2 + (x_R - x_{SO})^2 + (y_{RI} - y_S)^2} - x_R + x_{SO}\right|\right) \\ & + (x_R - x_{SI}) \\ & \times \ln\left(\left|\sqrt{a^2 + (x_R - x_{SI})^2 + (y_{RO} - y_S)^2} + y_{RO} - y_S\right|\right) \\ & + (y_S - y_{RO}) \\ & \times \ln\left(\left|\sqrt{a^2 + (x_R - x_{SI})^2 + (y_{RO} - y_S)^2} - x_R + x_{SI}\right|\right) \\ & + (y_{RI} - y_S) \\ & \times \ln\left(\left|\sqrt{a^2 + (x_R - x_{SI})^2 + (y_{RI} - y_S)^2} - x_R + x_{SI}\right|\right) \end{aligned} \tag{5}$$

$$\begin{aligned} m_B = {} & a\tan^{-1}\left(\frac{(x_R - x_{SO})(y_{RO} - y_S)}{a\sqrt{a^2 + (x_R - x_{SO})^2 + (y_{RO} - y_S)^2}}\right) \\ & - a\tan^{-1}\left(\frac{(x_R - x_{SO})(y_{RI} - y_S)}{a\sqrt{a^2 + (x_R - x_{SO})^2 + (y_{RI} - y_S)^2}}\right) \\ & - a\tan^{-1}\left(\frac{(x_R - x_{SI})(y_{RO} - y_S)}{a\sqrt{a^2 + (x_R - x_{SI})^2 + (y_{RO} - y_S)^2}}\right) \\ & + a\tan^{-1}\left(\frac{(x_R - x_{SI})(y_{RI} - y_S)}{a\sqrt{a^2 + (x_R - x_{SI})^2 + (y_{RI} - y_S)^2}}\right) \end{aligned} \tag{6}$$

$$m_C = -\gamma\,(y_{RO} - y_{RI})(x_{SO} - x_{SI}) \tag{7}$$

If two parallel conductors are considered, the procedure is essentially the same. There are some changes in the expressions for m_A, m_B and m_C as shown below. As in the previous scenario, both m_A and m_B are frequency independent and only m_C is a function of γ.

$$\begin{aligned} m_A = {} & (x_{RO} - x_{SO}) \\ & \times \ln\left(\left|\sqrt{a^2 + (x_{RO} - x_{SO})^2 + (y_S - y_R)^2} - x_{RO} + x_{SO}\right|\right) \\ & + (x_{SI} - x_{RO}) \\ & \times \ln\left(\left|\sqrt{a^2 + (x_{RO} - x_{SI})^2 + (y_S - y_R)^2} - x_{RO} + x_{SI}\right|\right) \\ & + (x_{SO} - x_{RI}) \\ & \times \ln\left(\left|\sqrt{a^2 + (x_{RI} - x_{SO})^2 + (y_S - y_R)^2} - x_{RI} + x_{SO}\right|\right) \\ & + (x_{RI} - x_{SI}) \\ & \times \ln\left(\left|\sqrt{a^2 + (x_{RI} - x_{SI})^2 + (y_S - y_R)^2} - x_{RI} + x_{SI}\right|\right) \end{aligned} \tag{8}$$

$$\begin{aligned} m_B = {} & \sqrt{a^2 + (x_{RO} - x_{SO})^2 + (y_S - y_R)^2} \\ & - \sqrt{a^2 + (x_{RO} - x_{SI})^2 + (y_S - y_R)^2} \\ & - \sqrt{a^2 + (x_{RI} - x_{SO})^2 + (y_S - y_R)^2} \\ & + \sqrt{a^2 + (x_{RI} - x_{SI})^2 + (y_S - y_R)^2} \end{aligned} \tag{9}$$

$$m_C = -\gamma\,(x_{RO} - x_{RI})(x_{SO} - x_{SI}) \tag{10}$$

where we have assumed that both segments (source and receiving) are not only parallel between them but also parallel to the y axis, i.e., $y_{RO} = y_{RI} = y_R$ and $y_{SO} = y_{SI} = y_S$; thus, $|y_R - y_S|$ is the distance between the segments.

The effect of the air–soil interface is included using the method of images, similar to Grcev and Grceva (2009), Arnautovski-Toseva and Grcev (2016). Thus, the elements in the impedance matrices are written as

$$\begin{aligned} Z_{T_{RS_{new}}} &= Z_{T_{RS}} + Z_{T_{RS_{image}}} \\ Z_{L_{RS_{new}}} &= Z_{L_{RS}} + Z_{L_{RS_{image}}} \end{aligned} \tag{11}$$

After the determination all the elements in the impedance matrices, the whole system is assembled in an equivalent nodal admittance of a given grounding system expressed by

$$\mathbf{Y}_g = \mathbf{e}_A^T \cdot \mathbf{Z}_T^{-1} \cdot \mathbf{e}_A + \mathbf{e}_B^T \cdot \mathbf{Z}_L^{-1} \cdot \mathbf{e}_B \tag{12}$$

where $\mathbf{e}_A$ and $\mathbf{e}_B$ are incidence matrices obtained by relating the nodes and adjacent electrodes.

3 Harmonic Impedance Evaluation

The harmonic impedance is evaluated by solving the following

$$\mathbf{Y}_g \cdot \mathbf{V} = \mathbf{I} \tag{13}$$

where $\mathbf{I}$ is null vector except at the node where the current injection occurs, which in this case is 1 A, and $\mathbf{V}$ represents the voltage rise at every node and the ground potential rise (GPR) at the point of injection. This procedure is then repeated for every frequency of interest giving the behavior of the GPR for a given grounding grid and a single injection point, and from the relation between the GPR and the injected current we obtain the harmonic impedance.

To illustrate the behavior of the proposed approach, we consider three grounding grids as depicted in Fig. 2. The data used for these tests are based on some of the configurations presented in Grcev and Heimbach (1997). All copper conductors have a 14 mm diameter and are buried at 0.5 m below ground surface. The current injection point is assumed to be at the lower left corner of the grounding grid. The frequency range of interest was from 100 Hz up to 2 MHz. The soil was represented using the frequency-dependent soil model proposed in Alipio and Visacro (2014). In this reference, there are three possibilities for considering the frequency dependence; we adopt the one associated with average results; more details in the soil modeling are presented in Appendix A. The frequency-dependent model relies heavily on the value of the low-frequency ground resistivity, ρ_0. So we have consider two main possibilities, a low resistivity ground at lower frequencies, i.e., $\rho_0 = 100\,\Omega \cdot$ m and one with higher resistivity, $\rho_0 = 1000\,\Omega \cdot$ m.

The results for the harmonic impedance are presented in Fig. 3. For the sake of comparison, we included the results for the harmonic impedance considering HEM. The mismatches between sHEM and HEM is presented as a dashed curve. It can be observed that there is a good agreement between the results, regardless of the configuration considered for a frequency below 200 kHz. We can observe that the highest mismatches occur for frequencies higher than 100 kHz and for more complex configurations, i.e., case #3. It can be observed that for a given configuration an increase in the soil resistivity leads to mismatches in higher frequencies.

Table 1 presents the RMSD (root mean squared deviation), calculated by (14), where N_f is the number of frequencies of the proposed approach when compared to HEM considering the distinct values of the low frequency resistivity, i.e., ρ_0. We have included the results considering only one term in the series expansion of the integrand, i.e., $n = 1$ which is equivalent to including only m_A and m_B in the closed-form expressions. We have also included the results considering a higher resistivity soil to further illustrate the behavior of the mismatch as a function of the ρ_0. It can be observed that sHEM increases the mismatch as ρ_0 increase. For lower values of ρ_0, we observe that both HEM and sHEM provide rather similar values. The approach considering only a single term has a lower accuracy independently of the value of ρ_0.

$$\text{RMSD} = \sqrt{\frac{\sum_{i=1}^{i=N_f} (\text{Z}_{\text{simplification}} - \text{Z}_{\text{trad. HEM}})^2}{N_f}} \tag{14}$$

Additionally, to analyze the relative error, Table 2 presents the MRE (maximum relative error), calculated by (15), where RE is the relative error when compared to HEM considering the distinct values of the low frequency resistivity. Similarly for the case of RMSD, for lower values of ρ_0 we observe that both HEM and sHEM provide rather similar values (with maximum error around 10%). It is important to highlight that the values presented in Table 2 is the worst case scenario, i.e., the maximum relative error in the frequency domain. Although one can find perceptual differences of the order of 20%, when considering a time-domain study, this differences tend to be reduced since it is a particular case for a particular frequency.

$$\text{RE} = 100 \frac{(\text{Z}_{\text{simplification}} - \text{Z}_{\text{trad. HEM}})}{\text{Z}_{\text{trad. HEM}}} \tag{15}$$

To have some prediction of the computational time of each formulation, a benchmark was done using 100 runs of each one. The median times are shown in Table 3 for building the frequency invariant "potential" matrices prior to the frequency loop and for one iteration of the loop that consists of correcting the matrices with the frequency terms and then solving the resulting linear system. The frequency of each run was chosen randomly between 10^2 and 10^7. The results show that HEM takes much more time to run than sHEM. Moreover, sHEM is still much faster to build even the "potential" matrices as it does not require numerically solving the integral.

4 Time-domain Results

We consider the evaluation of the ground potential rise (GPR) to assess the accuracy of the time responses associated with the proposed approach. Given an impulse current $i(t)$, the associated GPR can be determined as

$$\text{GPR} = \mathcal{F}^{-1}\left[Z(\omega)\,\mathcal{F}[i(t)]\right] \tag{16}$$

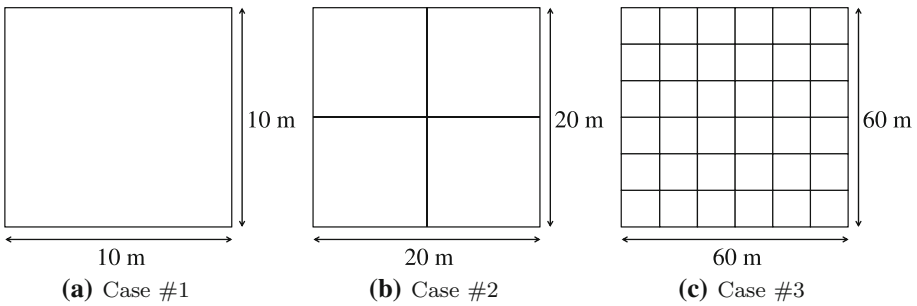

(a) Case #1 **(b)** Case #2 **(c)** Case #3

Fig. 2 Configurations for the grounding grid analysis

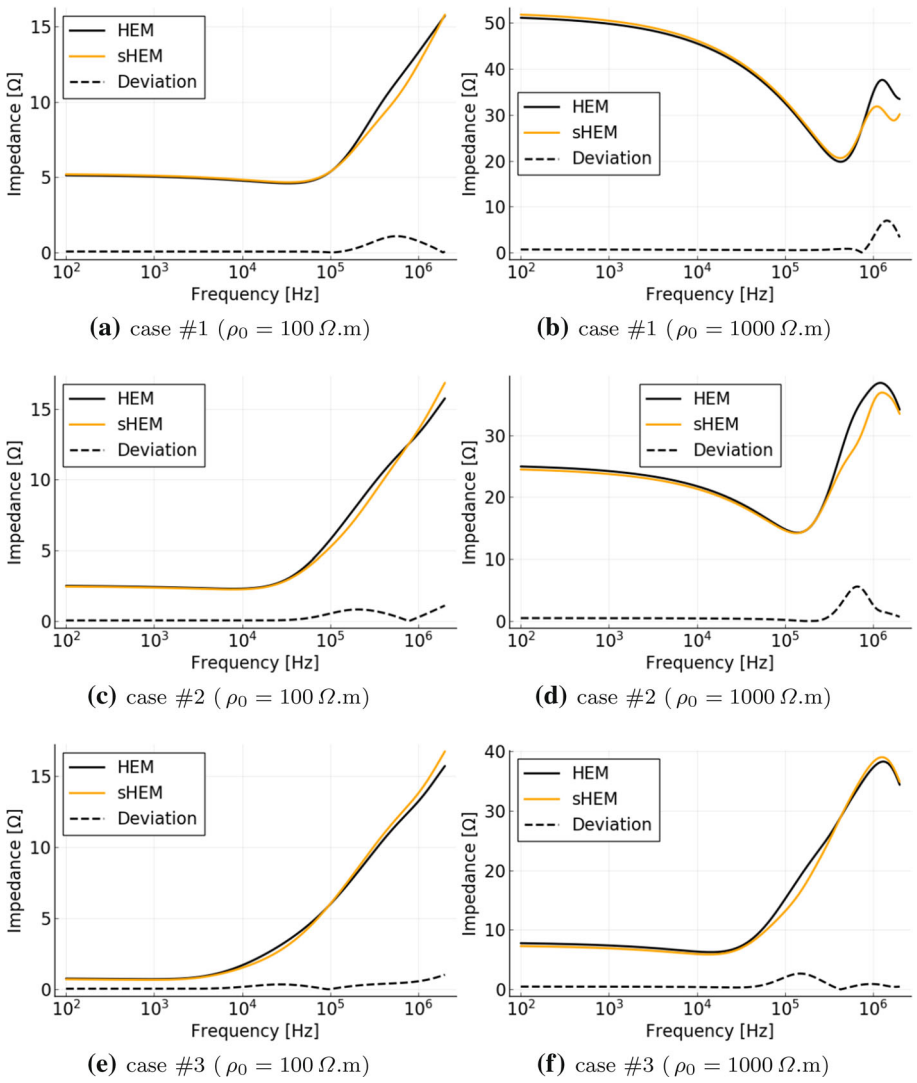

(a) case #1 ($\rho_0 = 100\,\Omega$.m) **(b)** case #1 ($\rho_0 = 1000\,\Omega$.m)

(c) case #2 ($\rho_0 = 100\,\Omega$.m) **(d)** case #2 ($\rho_0 = 1000\,\Omega$.m)

(e) case #3 ($\rho_0 = 100\,\Omega$.m) **(f)** case #3 ($\rho_0 = 1000\,\Omega$.m)

Fig. 3 Harmonic impedance for the three grounding grids considered

where $\mathcal{F}$ stands for the Fourier transform and $\mathcal{F}^{-1}$ its inverse. Two scenarios are considered here. The first one deals with the evaluation of the GPR for the three grounding grids presented in the previous section. In this case, we consider the same injection point as in the evaluation of the harmonic impedance. The second one is related to a comparison with an actual grounding system and its measured voltage.

4.1 Simulation Tests

For the simulation results, we consider two possibilities. In the first one, an impulse current associated with the first strokes measured at the San Salvatore Station Anderson and Eriksson (1980) is injected at the same point as where the harmonic impedance was calculated considering the three grounding grids of the previous section. The second one assumes that the injected current is related to the subsequent

Table 1 RMSD considering the distinct approaches

ρ_0 [Ω.m]	Case	sHEM	($n = 1$)
100	# 1	0.37466	2.06771
100	# 2	0.36601	2.06667
100	# 3	0.30455	2.05800
1000	# 1	1.66983	4.29428
1000	# 2	1.46316	4.48163
1000	# 3	0.93577	4.48886
2000	# 1	2.38862	5.17234
2000	# 2	2.10061	5.31356
2000	# 3	1.41390	5.32887

Table 2 Maximum relative error (MRE) considering HEM model as reference

ρ_0 [Ω.m]	Case	MRE [%]	Frequency [kHz]
100	# 1	−9.7795	496.4322
100	# 2	−10.6398	150.3636
100	# 3	−12.5536	17.6919
1000	# 1	−18.9898	1483.7157
1000	# 2	−16.4160	636.6871
1000	# 3	−14.6198	129.5099
2000	# 1	−23.5460	1722.6234
2000	# 2	−20.6947	739.2063
2000	# 3	−17.1982	174.5751

Table 3 Median computational burden for each approach

	Pre-loop	One freq. loop iteration
HEM	Non-applicable	8.257 s
sHEM	0.333 ms	0.939 ms

stroke also measured at the San Salvatore Station. In both cases, the current has the following expression

$$i(t) = \sum_{k=1}^{N} \frac{I_k}{\eta_k} \exp(-t/\tau_{2k}) \left[\frac{(t/\tau_{1k})^{n_k}}{1 + (t/\tau_{1k})^{1/n_k}} \right] \tag{17}$$

where the values of N, I_k, η_k, τ_{1k}, τ_{2k}, and n_k for both first and subsequent strokes can be found in de Conti and Visacro (2007). Figure 4 depicts the waveform of first and subsequent stroke currents considered in the analysis.

Considering the first stroke current, the results are depicted in Fig. 5. It can be observed that apart from minor mismatches around the maxima of the GPR, the results of sHEM are rather close to the ones found using HEM. The highest deviations occur around the peak value of the voltage. The mismatches between sHEM and HEM are presented as a dashed line. Figure 6 presents the results considering the subsequent stroke,

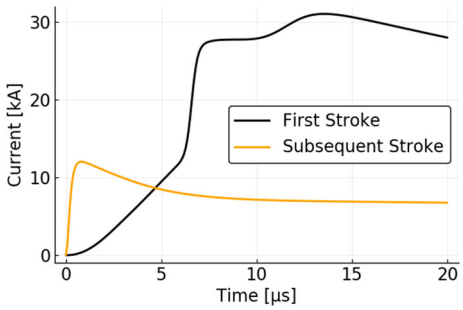

Fig. 4 Waveform of injected current considering first and subsequent strokes

Table 4 Peak relative error (PRE) considering HEM model as reference

ρ_0 [Ω.m]	Case	$\text{PRE}_{\text{First}}$ [%]	$\text{PRE}_{\text{Subsequent}}$ [%]
100	# 1	−3.2525	−6.8624
100	# 2	−6.2486	−6.9232
100	# 3	−4.4699	−1.3278
1000	# 1	1.3653	1.4557
1000	# 2	−2.0136	−8.3173
1000	# 3	−6.7430	−5.5350
2000	# 1	1.3514	1.4057
2000	# 2	−1.9809	−10.0660
2000	# 3	−6.9213	−6.0585

which is a waveform which presents a larger frequency spectrum than the one found in the first strokes. The idea of this test is to excite higher frequencies to assess the behavior of sHEM in the case of fast front waves. A similar behavior was found in this test. Again, a good agreement between the results is found, and a similar behavior of sHEM when compared with HEM was found.

To systematically analyze the relative error, Table 4 presents the PRE (peak relative error), i.e., the relative error considering the maximum value of GPR [calculated by (18)]. Averagely, for subsequent strokes, we observe higher differences. However, in both cases (first and subsequent) the perceptual differences are relatively low, with maximum error around 10%.

$$\text{PRE} = 100 \frac{(\max(\text{GPR}_{\text{simplification}}) - \max(\text{GPR}_{\text{trad. HEM}}))}{\max(\text{GPR}_{\text{trad. HEM}})} \tag{18}$$

4.2 Experimental Validation

A final comparison was carried out considering an actual grounding grid. In this work, we considered the arrangement tested in Visacro et al. (2015) to verify the accuracy of the proposed formulation presented here. This case was used since it

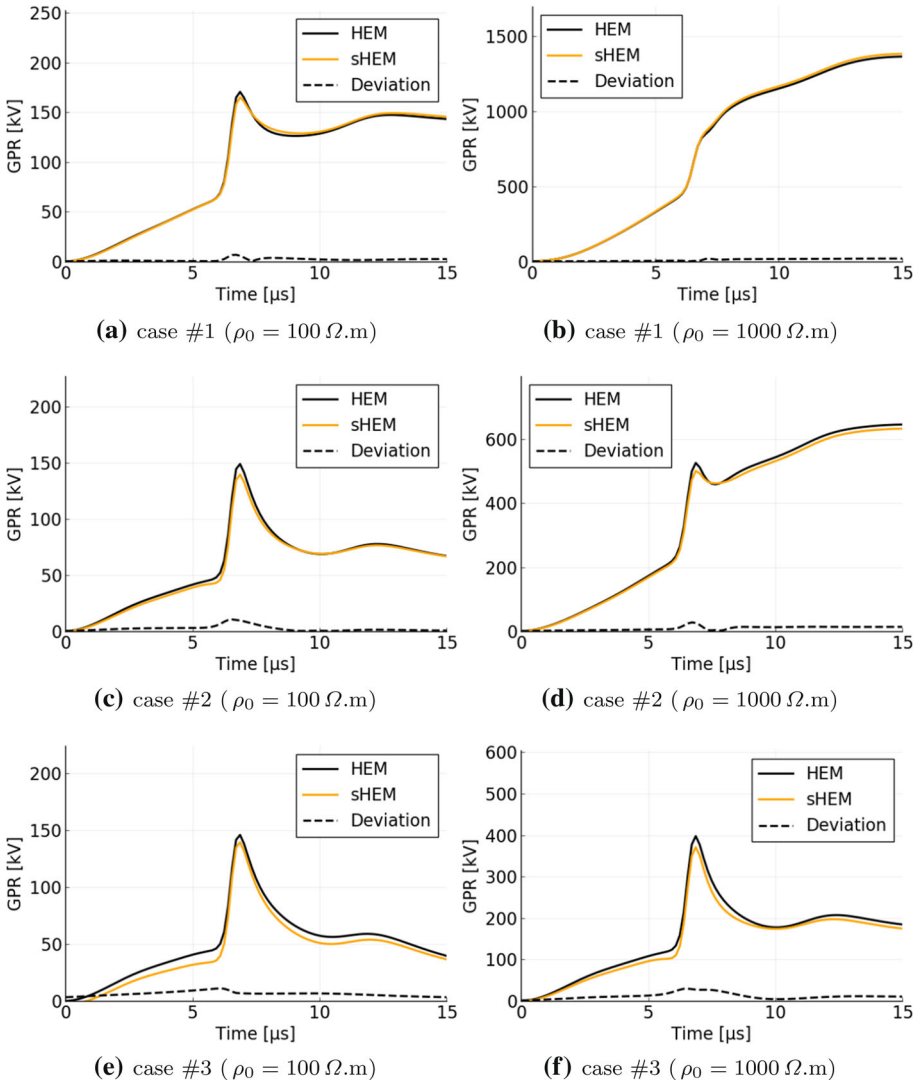

Fig. 5 GPR responses considering first stroke impulse current

corresponds to a complex grounding arrangement and, therefore, allows to give more generality to the proposed model. The tested grounding system consists of a rectangular grid of 16 m × 20 m, composed by 20 regular meshes of 4 m × 4 m. The conductors are constructed from steel-galvanized alloys with a 0.5-cm radius. The grid is buried at a depth of 0.5 m in a soil of apparent resistivity of 2000 $\Omega \cdot m$. Independent measurements were performed in field conditions to determine the frequency dependence of soil resistivity and permittivity. A schematic of the tested grounding grid and experimental setup is depicted in Fig. 7.

Two types of currents were injected in the grounding grid: one with a zero-to-peak rise time of 0.7 μs and the other with 4 μs. These currents were named fast front (ff) and slow front (sf), respectively, and were injected at the center and corner of the grid. Figure 8 depicts these two currents. The injected current was determined by measuring the current in R_s as shown in Fig. 7. The impressed current and the developed GPR with respect to remote earth at the current injected point were measured using a two-channel oscilloscope. It is to be noted that the injected current is determined from the voltage drop across the resistor RS shown in Fig. 7. To avoid electromagnetic coupling between the cables used in the measurements, the potential and current circuits were laid orthogonal from each other. Further details of the design and characterization of the measurement setup system can be found in Visacro et al. (2015).

Figure 9 shows GPR for both the experimental setup and the simulation results using the proposed approach considering both slow and fast front currents. Again, a good agreement was found considering both current pulses and injection points. The observed differences are within the inherent uncertainties of measurements. Interestingly, in the case of fast fronted pulse, the peak of the developed GPR for the current injection in the grid corner is slightly higher in comparison with the GPR for the injection in the grid center.

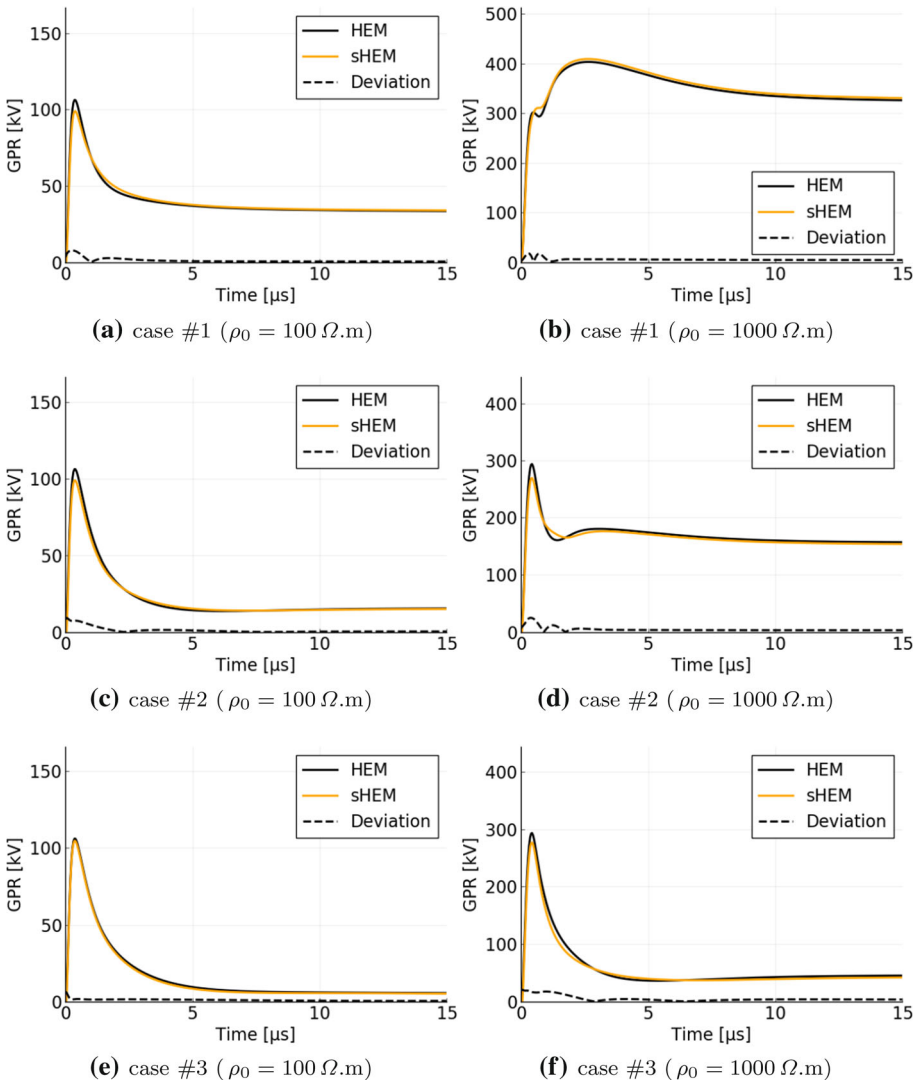

Fig. 6 GPR responses considering subsequent strokes

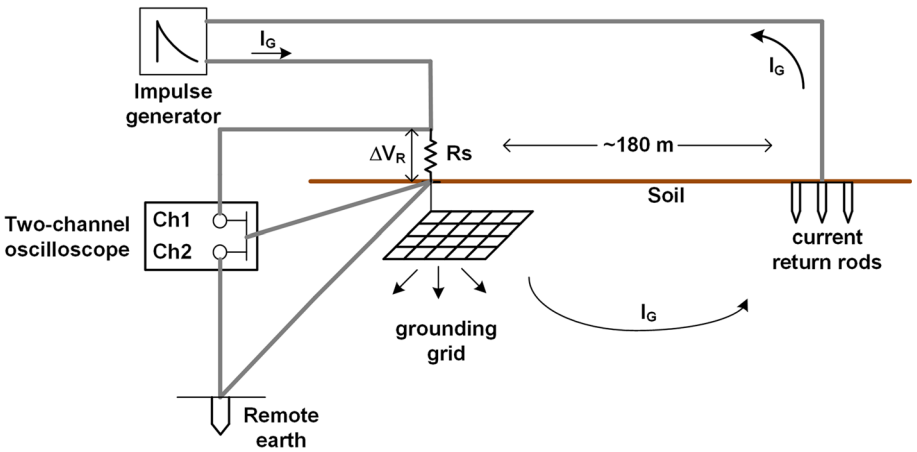

Fig. 7 Experimental setup

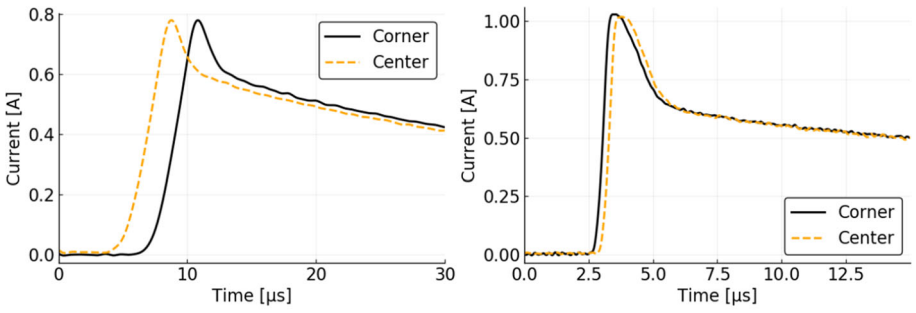

Fig. 8 Experimental injected current in the grounding grid

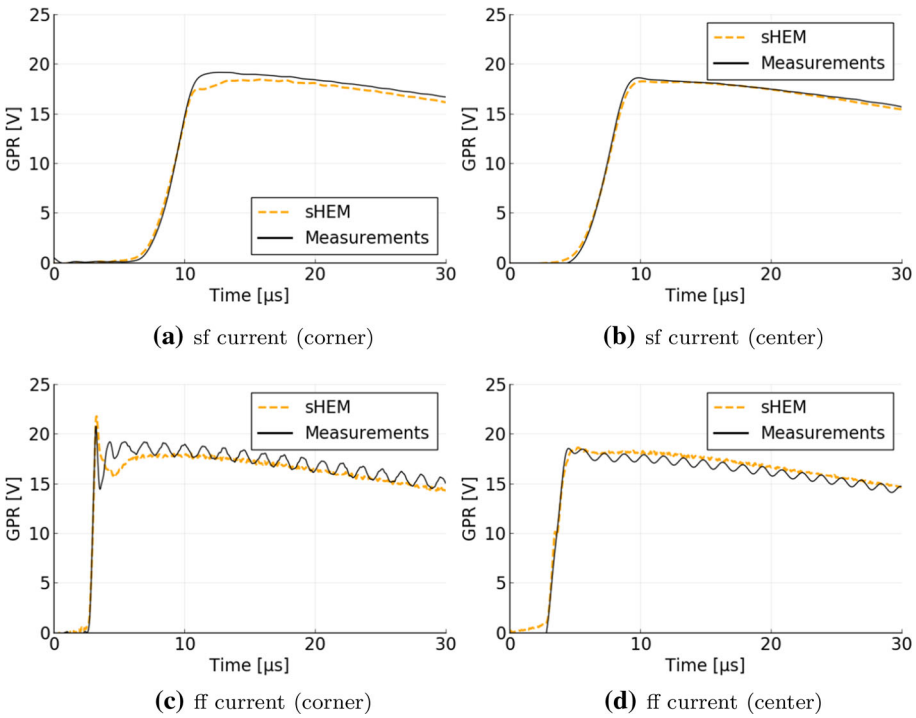

Fig. 9 GPR comparison with experimental results

This stems from the fact that, for the faster current pulse, the effective area seen from the corner is smaller than that seen from the center, which results in a higher GPR peak. It is also interesting to note that there is a greater difference between the measured and simulated GRPs for injection in the corner in relation to the case of injection in the center, for both current pulses, fast and slow. It seems that this fact is associated with the greater symmetry of conductors around the current injection point in the center of the grid, where in this case the approaches proposed in the paper are more adherent. However, it should be noted that the difference in question is, in practical terms, small, which does not affect the validation of the formulations proposed in the paper. Considering the good accordance between simulated and experimental results, it is seen that the proposed approach captures well this complex dynamic period of the transient response of the grounding grid. Accordingly to Visacro et al. (2015), a spurious signal in soil during the measurements is responsible for the oscillations in the tail of the measured GPR in response to the faster current pulse and for the differences between simulated and experimental results in the tail part of the curve.

5 Discussion

The proposed approach, sHEM, has outperformed HEM in all test cases considering the computational time. Moreover, sHEM presented a good agreement with experimental results. The RMSD associated with using the sHEM simplification increases in soils having high and constant electrical resistivity.

The usage of two terms in the series expansion allowed to an improved numerical performance when compared with a simpler approach using only the first term of the series expansion. This additional term is directly related to the prop-

agation function γ and does not compromise the numerical performance of sHEM in the frequency loop.

Even though the focus of this paper has been in grounding grids, thus involving orthogonal or parallel conductors, the approach proposed in sHEM can be adapted to represent conductor at distinct angles between them. Therefore, sHEM could be used for the modeling of counterpoise. This investigation is left for future work.

As it is well known, the numerical performance of methods such as HEM or PEEC depends heavily on the number of segments used to represent a given conductor. In sHEM, the scenario is rather distinct as an increase in the number of segments does not affect significantly the numerical performance. The exception being where there is a very large number of segments, as in this scenario the computational time associated with the impedance matrices evaluation becomes irrelevant when compared with the time associated with solving the linear system. In general, as it was shown here, the computational cost of the impedance evaluation in sHEM is rather small. Furthermore, it was found out that as the number of segments increases, the numerical performance of sHEM improves.

6 Conclusions

This paper investigates the adequacy of using two terms in the series expansion of the finite integral used in the transient analysis of grounding system. This allows to use a closed-form approximation of the integral, thus avoiding any numerical issues related to the evaluation of high oscillating complex integrals. Furthermore, the obtained expressions are rather simple, with a larger part of it being processed prior to entering the frequency loop, thus improving the numerical performance of the proposed approach.

The comparison with simulation results using HEM indicates that in the lower frequency range, sHEM responses are very close to the results obtained with HEM approaches. The comparison with experimental results showed that a suitable accuracy is found using sHEM. Future work will deal with the application of sHEM in sensitivity analysis for practical assessment of actual grounding grids.

Acknowledgements This study was financed in part by the Coordenação de Aperfeiçoamento de Pessoal de Nível Superior–Brasil (CAPES), Finance Code 001. It also was partially supported by INERGE (Instituto Nacional de Energia Elétrica), CNPq (Conselho Nacional de Desenvolvimento Científico e Tecnológico) FAPEMIG (Fundação de Amparo à Pesquisa do Estado de Minas Gerais) and FAPERJ (Fundação Carlos Chagas Filho de Amparo à Pesquisa do Estado do Rio de Janeiro).

A Frequency-Dependent Soil Modeling

There are several experimentally obtained formulas for modeling the frequency dependence of soil parameters. In this paper, the Alipio–Visacro model is considered, which is based on the measurement of the frequency response of 65 type of soils, which presented low-frequency resistivity values ranging from 60 to about $18,000\,\Omega\cdot$ m Alipio and Visacro (2014). This model satisfies causality and was recently suggested in the CIGRE Brochure to take into account the frequency dependence of soil parameters in lightning related studies C4.33 (2019). According to Alipio–Visacro soil model, the soil is represented by an immittance given by

$$\kappa(\omega) = \sigma_e(\omega) + j\omega\varepsilon_e(\omega) \tag{19}$$

where the effective soil conductivity, $\sigma_e(\omega)$ (10^{-3} S/m), and permittivity, $\varepsilon_e(\omega)$ (F/m) can be calculated using the following

$$\begin{aligned}\sigma_e(\omega) &= \sigma_0\left[1 + h\cdot\left(\frac{\omega}{2\pi\,10^6}\right)^{\xi}\right]\\ \varepsilon_e(\omega) &= \varepsilon_\infty + \frac{\tan(\xi\pi/2)\cdot 10^{-3}}{2\pi\,\varepsilon_0 10^{6\xi}}\sigma_0\cdot h\cdot\left(\frac{\omega}{2\pi}\right)^{\xi-1}\end{aligned} \tag{20}$$

where $\sigma_0 = 1/\rho_0$ is the low-frequency soil conductivity, $\varepsilon_\infty = c\,\varepsilon_0$. The value of c and h are chosen depending of the natural statistical dispersion of the frequency dependence of soil parameters. In this work, we adopt the mean model which implies $\varepsilon_\infty = 12\,\varepsilon_0$ and $h = 1.26\cdot\sigma_0^{-0.73}$.

References

Akbari, M., Sheshyekani, K., & Alemi, M. R. (2013). The effect of frequency dependence of soil electrical parameters on the lightning performance of grounding systems. *IEEE Transactions on Electromagnetic Compatibility*, *55*(4), 739–746.

Alipio, R., Conceição, D., Dias, R. N., Visacro, S., & Yamamoto, K. (2017). The effect of frequency dependence of soil electrical parameters on the lightning performance of typical wind-turbine grounding systems. In 2017 international symposium on lightning protection (xiv sipda) (pp. 353- 358). IEEE.

Alipio, R., Conceição, D., de Conti, A., Yamamoto, K., Dias, R. N., & Visacro, S. (2019). A comprehensive analysis of the effect of frequency-dependent soil electrical parameters on the lightning response of wind-turbine grounding systems. *Electric Power Systems Research*, *175*, 105927.

Alipio, R., & Visacro, S. (2014). Modeling the frequency dependence of electrical parameters of soil. *IEEE Transactions on Electromagnetic Compatibility*, *56*(5), 1163–1171.

Anderson, R. B., & Eriksson, A. J. (1980). Lightning parameters for engineering application. *Electra*, *69*, 65–102.

Arnautovski-Toseva, V., & Grcev, L. (2016). On the image model of a buried horizontal wire. *IEEE Transactions on Electromagnetic Compatibility*, *58*(1), 278–286.

C4.33, W.-G. (2019). Impact of soil-parameter frequency dependence on the response of grounding electrodes on the lightning performance of electrical systems. CIGRE.

CIGR. (2019). Electromagnetic computation methods for lightning surge studies with emphasis on the FDTD method (Technical Brochures No. 785). Cigré. WG C4.37.

de Conti, A., & Visacro, S. (2007). Analytical representation of single- and double-peaked lightning current waveforms. *IEEE Transactions on Electromagnetic Compatibility*, *49*(2), 448–451.

Grcev, L., & Dawalibi, F. (1990). An electromagnetic model for transients in grounding systems. *IEEE Transactions on Power Delivery*, *5*(4), 1773–1781. https://doi.org/10.1109/61.103673.

Grcev, L., & Grceva, S. (2009). On HF circuit models of horizontal grounding electrodes. *IEEE Transactions on Electromagnetic Compatibility*, *51*(3), 873–875.

Grcev, L. D., & Heimbach, M. (1997). Frequency dependent and transient characteristics of substation grounding systems. *IEEE Transactions on Power Delivery*, *12*(1), 172–178. https://doi.org/10.1109/61.568238.

Grcev, L., Kuhar, A., Arnautovski-Toseva, V., & Markovski, B. (2018). Evaluation of high-frequency circuit models for horizontal and vertical grounding electrodes. *IEEE Transactions on Power Delivery*, *33*(6), 3065–3074. Closed-Form Approximation for Grounding Grids Transient Analysis 19.

Kuhar, A., Arnautovski-Toševa, V., & Grčev, L. (2017). High frequency enhancement of the hybrid electromagnetic model by implementing complex images. *Journal of Electrical Engineering and Information Technologies*, *2*(2), 79–87.

Kuhar, A., Arnautovski-Toševa, V., Ololoska-Gagoska, L., Grčev, L., & Markovski, B. (2018). Influence of segmentation on the precision of circuit based methods. *Journal of Electrical Engineering and Information Technologies*, *3*(1–2), 21–30.

Lima, A. C. S., Moura, R. A. R., Vieira, P. H. N., Schroeder, M. A. O., & Correia de Barros, M. T. (2019a). Implementing hybrid electromagnetic models in time-domain simulations. In International conference on power system transients (IPST 2019), Perpignan, France. https://www.ipstconf.org/.

Lima, A. C. S., Moura, R. A. R., Vieira, P. H. N., Schroeder, M. A. O., & de Barros, M. T. C. (2019b). A computational improvement in grounding systems transient analysis. *IEEE Transactions on Electromagnetic Compatibility*,. https://doi.org/10.1109/TEMC.2019.2918621.

Liu, Y., Theethayi, N., & Thottappillil, R. (2005). An engineering model for transient analysis of grounding system under lightning strikes: Nonuniform transmission-line approach. *IEEE Transactions on Power Delivery*, *20*(2), 722–730. https://doi.org/10.1109/TPWRD.2004.843437.

Menter, F., & Grcev, L. (1994). Emtp-based model for grounding system analysis. *IEEE Transactions on Power Delivery*, *9*(4), 1838–1849. https://doi.org/10.1109/61.329517.

Moura, R. A. R., Schroeder, M. A. O., Lima, A. C. S., & Vieira, P. H. N. (2020). Closed-form approximation for horizontal grounding electrodes transient analysis. Journal of Control, Automation and Electrical Systems (JCAE). https://doi.org/10.1007/s40313-020-00592-x

Ruehli, A. (1996). Partial element equivalent circuit (PEEC) method and its application in the frequency and time domain. In Proceedings of symposium on electromagnetic compatibility (pp. 128-133). IEEE.

Ruehli, A. (1974). Equivalent circuit models for three-dimensional multiconductor systems. *IEEE Transactions on Microwave Theory and Techniques*, *22*(3), 216–221.

Schroeder, M. A. O., Moura, R. A. R., & Machado, V. M. (2020). A discussion on practical limits for segmentation procedures of tower-footing grounding modeling for lightning responses. *IEEE Transactions on Electromagnetic Compatibility*,. https://doi.org/10.1109/TEMC.2020.2982358.

Silveira, F., Visacro, S., Herrera, J., & Torres, H. (2009). Evaluation of lightninginduced voltages over a lossy ground by the hybrid electromagnetic model. *IEEE Transactions on Electromagnetic Compatibility*, *51*(1), 156–160.

Sunde, E. D. (1968). *Earth conduction effects in transmission systems*. New York: Dover.

Tanabe, K. (2001). Novel method for analyzing dynamic behavior of grounding systems based on the finite-difference time-domain method. *IEEE Power Engineering Review*, *21*(9), 55–57.

Tsumura, M., Baba, Y., Nagaoka, N., & Ametani, A. (2006). FDTD simulation of a horizontal grounding electrode and modeling of its equivalent circuit. *IEEE Transactions on Electromagnetic Compatibility*, *48*(4), 817–825.

Visacro, S. & Portela, C. M. (1992). Modelling of earthing systems for lightning protection applications, including propagation effects. In 21st international conference on lightning protection (iclp) (pp. 129-132). Berlin.

Visacro, S., Alipio, R., Pereira, C., Guimarães, M., & Schroeder, M. A. O. (2015). Lightning response of grounding grids: Simulated and experimental results. *IEEE Transactions on Electromagnetic Compatibility*, *57*(1), 121–127.

Visacro, S., Alipio, R., Vale, M. H. M., & Pereira, C. (2011). The response of grounding electrodes to lightning currents: The effect of frequencydependent soil resistivity and permittivity. *IEEE Transactions on Electromagnetic Compatibility*, *53*(2), 401–406.

Visacro, S., & Soares, A. (2005). HEM: A model for simulation of lightning related engineering problems. *IEEE Transactions on Power Delivery*, *20*(2), 1206–1208. https://doi.org/10.1109/TPWRD.2004.839743.

Yamamoto, K., Yanagawa, S., Yamabuki, K., Sekioka, S., & Yokoyama, S. (2010). Analytical surveys of transient and frequency-dependent grounding characteristics of a wind turbine generator system on the basis of field tests. *IEEE Transactions on Power Delivery*, *25*(4), 3035–3043.

Yutthagowith, P., Ametani, A., Nagaoka, N., & Baba, Y. (2011). Application of the partial element equivalent circuit method to analysis of transient potential rises in grounding systems. *IEEE Transactions on Electromagnetic Compatibility*, *53*(3), 726–736.

Publisher's Note Springer Nature remains neutral with regard to jurisdictional claims in published maps and institutional affiliations.